CMS Physics Analysis Summary

Contact: cms-phys-conveners-ftr@cern.ch 2018/12/14

Study of the expected sensitivity to the P'_5 parameter in the $B^0 \to K^{*0}\mu^+\mu^-$ decay at the HL-LHC

The CMS Collaboration

Abstract

The expected sensitivity to the P'_5 parameter in $B^0 \to K^{*0}\mu^+\mu^-$ decays from an integrated luminosity of 300 and 3000 fb^{-1} of pp collisions at a center-of-mass energy of 14 TeV at the HL-LHC is presented. Angular observables in the $B^0 \to K^{*0}\mu^+\mu^-$ decay, such as the P'_5 parameter, are of particular interest as their theoretical predictions are less affected by hadronic uncertainties. With an integrated luminosity of 3000 fb^{-1}, the uncertainties on the shape of the P'_5 parameter will improve by up to a factor of 15, depending on the dimuon mass squared region, compared to the published results from 20 fb^{-1} at 8 TeV.

1 Introduction

The high-luminosity upgrade of the CERN LHC accelerator (HL-LHC) and the detectors will allow for the collection of an unprecedented amount of data. The expected integrated luminosity of 3000 fb^{-1} during 10 years of operation [1] will provide the ability to perform precision studies of rare decays of b hadrons. In particular, the $B^0 \to K^{*0}(K^+\pi^-)\mu^+\mu^-$ channel, whose branching ratio is at the level of 10^{-7}, can be used to precisely measure important angular parameters, including the so-called P'_5 variable [2, 3].

The differential decay rate for the $B^0 \to K^{*0}\mu^+\mu^-$ channel can be written in terms of the dimuon invariant mass squared q^2 and three angular variables as a combination of spherical harmonics, weighted by q^2-dependent angular parameters. These angular parameters in turn depend upon complex decay amplitudes, which are described by Wilson coefficients in the Effective Field Theory (EFT) Hamiltonian. The LHCb Collaboration reported a discrepancy of about 3 standard deviations with respect to the standard model (SM) predictions for the parameter P'_5 [4], the Belle Collaboration reported a discrepancy almost as large [5], and CMS recently published a value consistent with the SM [6]. More precise measurements are needed to understand the tension between the measurements and the SM predictions. This measurement gains particular interest when considered in the more general framework of the "flavor anomalies", that suggest a possibility of Lepton Flavour Universality Violation [7].

The HL-LHC conditions present particular challenges for the collection, reconstruction, and analysis of b hadron decays. With an average of 200 proton-proton (pp) collisions per bunch crossing (pileup), the reconstruction of the relatively low-momentum charged tracks from b hadron decays and the assignment of the tracks to the correct vertex becomes quite challenging. In addition, being able to trigger on relatively low momentum muons, with the associated high data rate can be problematic.

On the other hand, the CMS detector will undergo many upgrades to handle the HL-LHC conditions. The relevant upgrades for this analysis are a new silicon tracker with finer granularity, extended coverage, and better radiation tolerance, improvements to the muon system, the ability to reconstruct and use tracks in the first stage of the trigger, and a data-acquisition system to allow for many more events to be stored. These improvements are designed to ensure that the CMS performance meets or exceeds the original performance even in the harsh environment of the HL-LHC. A detailed overview of the CMS detector upgrade program is presented in Ref. [8–10], while the expected performance of the reconstruction algorithms and pile-up mitigation with the CMS detector is summarized in Ref. [11].

In this paper the sensitivity for the measurement of the P'_5 parameter at HL-LHC is estimated. Starting from the existing CMS measurement [6] obtained from 8 TeV pp collision data, we use the expected improvements of the statistical and systematic uncertainties assuming a center-of-mass energy of 14 TeV and integrated luminosity of 3000 fb^{-1} to obtain the expected precision on P'_5 at the end of the HL-LHC period.

2 Summary of previous analysis

The CMS analysis of Run I data [6] is based on an integrated luminosity of 20 fb^{-1}, collected at $\sqrt{s} = 8$ TeV in 2012. The analysis measures the P'_5 variable of the $B^0 \to K^{*0}\mu^+\mu^-$ decay as a function of q^2 in the range from 1 to 19 GeV^2. CMS had previously exploited the same data set to measure two other angular parameters in the $B^0 \to K^{*0}\mu^+\mu^-$ decay as a function of q^2, the forward-backward asymmetry of the muons, A_{FB}, and the K^{*0} longitudinal polarization frac-

tion, F_L, as well as the differential branching fraction, $d\mathcal{B}/dq^2$ [12]. The decay is fully described as a function of the three angles θ_ℓ, θ_K and ϕ, where θ_ℓ is the angle between the momentum of the positive (negative) muon and the direction opposite to the B^0 ($\overline{B}^0$) in the dimuon rest frame; θ_K is the angle between the kaon momentum and the direction opposite to the B^0 ($\overline{B}^0$) in the K^{*0} ($\overline{K}^{*0}$) rest frame; ϕ is the angle between the dimuon and the $K^+\pi^-$ decay planes in the B^0 rest frame. The expression describing the angular distribution can be found in Ref. [6]. The possible contribution from spinless (S-wave) $K^+\pi^-$ combinations is taken into account in the decay description with three terms: F_S, which is related to the S-wave fraction, and A_S and A_S^5, which are the interference amplitudes between the S-wave and P-wave decays. The observables of interest are extracted for each q^2 bin from an unbinned extended maximum likelihood fit to $m(\mu^+\mu^-K^+\pi^-)$ and the three angular variables.

In this analysis the CP state assignment is of great importance because the angular observables behave oppositely for each one of the two CP eigenstates. In absence of a particle ID detector, and given that the ionization energy loss method for hadron identification is not applicable to the kinematic range of the particles involved in this process [13], the four-track candidate is identified as a B^0 or $\overline{B}^0$ based on the $K^+\pi^-$ or $K^-\pi^+$ invariant mass being closest to the nominal K^{*0} mass. The fraction of candidates assigned to the incorrect state is estimated from the simulation to vary between 12 and 14% among the different q^2 bins.

The probability density function takes into account correctly and wrongly tagged signal events, background events, and the efficiency in the three angular variables. The efficiency, which is the product of the acceptance of the detector and the trigger, reconstruction, and selection efficiencies, is obtained from a Monte Carlo (MC) simulation, which reproduces the data taking conditions. It is determined, for each q^2 bin, as a function of the three angles $\cos\theta_\ell$, $\cos\theta_K$ and ϕ.

The resonant $B^0 \to J/\psi K^{*0}$ and $B^0 \to \psi' K^{*0}$ decays are used as control channels (corresponding to the q^2 bins 8.68 – 10.09 and 12.90 – 14.18 GeV^2). Here, ψ' denotes the $\psi(2S)$ meson.

The online event selection uses a hardware low-p_T dimuon trigger and a High Level Trigger (HLT) selection based on the dimuon invariant mass and the compatibility of the two muons with a common vertex displaced from the pp collision region. The offline reconstruction requires that two oppositely charged muons and two oppositely charged hadrons are fit to a common vertex, and satisfy the set of kinematic and topological requirements described in Ref. [6]. In case multiple B^0 candidates per event are found, only the one with the largest χ^2 fit probability is retained.

Contamination from the resonant $B^0 \to J/\psi K^{*0}$ and $B^0 \to \psi' K^{*0}$ decays is reduced using a combined selection on $m(\mu^+\mu^-)$ and $m(\mu^+\mu^-K^+\pi^-)$, i.e., rejecting events for which the condition $|(m(\mu^+\mu^-K^+\pi^-) - m(B^0)_{\rm PDG}) - (m(\mu^+\mu^-) - m(J/\psi \text{ or } \psi')_{\rm PDG})| \leq R_{rej}$ is satisfied. The R_{rej} value and the use of $m(J/\psi)_{\rm PDG}$ versus $m(\psi')_{\rm PDG}$ [14] depend on the $m(\mu^+\mu^-)$ analyzed region [6].

3 Extrapolation to the HL-LHC

In order to extrapolate from the Run I results, some assumptions are made. We have not considered the effects of improvements in the analysis strategy (for instance the use of different selection criteria or fits). We have assumed that the trigger thresholds and efficiencies will remain the same. In fact, this is likely to be a conservative assumption as the availability of tracking information at the first level of the trigger may result in a higher efficiency than in

Run I. The extrapolation method assumes that the signal-to-background is the same. Except as noted below regarding the mass resolution, this is expected to be the case as the primary source of background is from other b decays, whose cross section scales the same as the signal. Samples of simulated signal events were used to evaluate the effect of three important aspects of the analysis: mass resolution, CP mistagging rate, and the effect of pileup in order to justify the extrapolation method.

3.1 Mass resolution

For analyses with significant background, the mass resolution is an important aspect in obtaining a high signal to background. The left plot of Fig. 1 shows the $K^+\pi^-\mu^+\mu^-$ invariant mass distribution in a specific q^2 bin for the Run I and Phase-2 simulations, and the width of the B^0 signal for each q^2 bin is shown on the right. The width is measured by performing a fit to the $K^+\pi^-\mu^+\mu^-$ mass distribution in each q^2 bin, parametrizing the B^0 signal with the sum of two Gaussian distributions and taking the average of the two Gaussian widths (weighted by their relative contribution) as the B^0 width. The improvement in mass resolution with the Phase-2 conditions should improve the signal-to-background ratio from the Run I result. This improvement is not included in the extrapolation.

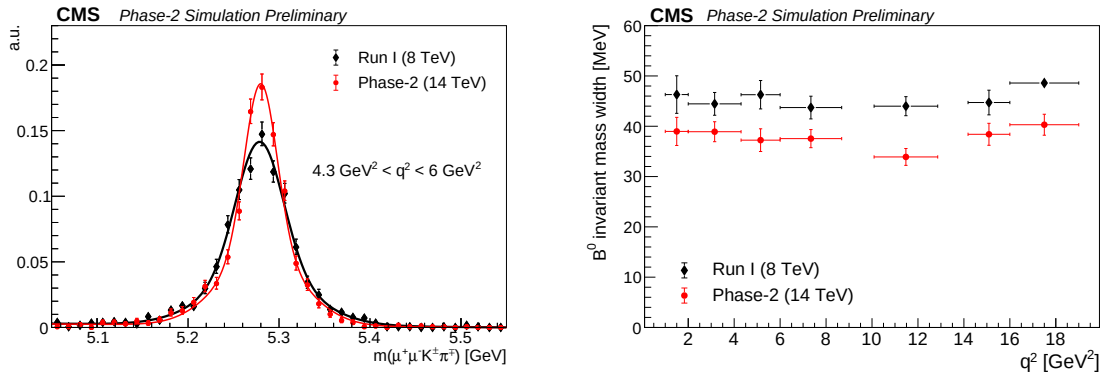

Figure 1: Left: the $K^+\pi^-\mu^+\mu^-$ invariant mass distribution for bin 2 from Run I (black diamonds) and Phase-2 (red circles) simulation. A fit with the sum of two Gaussian functions is superimposed to each distribution. Right: the B^0 signal width for each q^2 bin in the Run I and Phase-2 simulations.

3.2 Mistag rate

The assignment of the CP state is based on the distance of the invariant mass of the two hadrons from the K^{*0} PDG mass [14]. Both mass hypotheses are computed, i.e. $K^+\pi^-$ and $K^-\pi^+$, but only the one closest to the K^{*0} world average mass is retained, which also directly determines the CP state of the mother meson. The CP mistag fraction, defined as the ratio between the number of wrongly tagged events and the total number of signal events, is determined from simulation by counting the number of correctly and wrongly tagged events, where only truth-matched events passing all of the selection criteria are considered. The mistag fraction obtained from the Phase-2 MC simulation is found to be the same as in Run I.

3.3 Pileup effects

The analysis performance was proven not to be significantly affected by pileup during the studies performed for the previous publications [6, 12]. In particular, the event selection re-

quirements do not depend on the primary vertex choice or utilize isolation information. Furthermore, requiring that each track in the decay have a distance of closest approach to the beamspot greater than 2 standard deviations helps to reduce the contamination from tracks originating from pileup vertices.

In order to have a more quantitative estimation of possible pileup effects, we compared the distributions of the more relevant variables between the samples with and without pileup: no significant degradation of the discriminating power was observed.

3.4 Expected yield and statistical uncertainty

For each q^2 bin, the expected $B^0 \to K^{*0}\mu^+\mu^-$ signal yields are obtained from a sample of simulated signal events generated with the Phase-2 conditions, including an average of 200 pileup. The yields in each q^2 bin are obtained from an extended unbinned maximum likelihood fit to the $K^+\pi^-\mu^+\mu^-$ invariant mass, parameterizing the signal with the sum of two Gaussian distributions and the (negligible) background with an exponential distribution. All parameters are freely varying in the fit. The yields are weighted by the trigger efficiencies measured in the Run I sample and scaled to luminosities of 300 and 3000 fb^{-1}. The total expected number of $B^0 \to K^{*0}\mu^+\mu^-$ signal events, excluding the q^2 regions associated with the resonant decays, is around 700K for an integrated luminosity of 3000 fb^{-1}. The estimated statistical uncertainty on the P_5' parameter is obtained by scaling the statistical uncertainty measured in Run I by the square root of the ratio between the yields observed in the Run I data and the Phase-2 simulation:

$$\sigma_{P_5'}^{Phase2} = \sqrt{\frac{N^{RunI}}{N^{Phase2}}}\sigma_{P_5'}^{RunI} \tag{1}$$

4 Systematic uncertainties

The systematic uncertainties are also extrapolated from the Run I analysis. Improved understanding of theory and the experimental apparatus is expected to reduce many uncertainties by a factor of 2 in the Phase-2 scenario. These uncertainties are those related to contamination from resonant decays, signal mass shape, CP mistagging rate, efficiency, angular resolution, and other simulation modeling. The uncertainty on the description of the background mass distribution, the one associated with the propagation of the uncertainty on F_L, F_S and A_S, and the fit bias introduced by the fitting procedure depend on the available amount of data. These uncertainties are therefore scaled the same as the statistical uncertainties. The uncertainty related to the limited number of simulated events is neglected, under the assumption that sufficiently large simulation samples will be available by the time the HL-LHC becomes operational.

5 Results

The Run I results and the projected statistical uncertainties and total uncertainties (statistical and systematic uncertainties added in quadrature) in each q^2 bin are shown in Figs. 2 and 3 for an integrated luminosity of 300 and 3000 fb^{-1}, respectively. The statistical and systematic uncertainties from Run I and for an integrated luminosity of 3000 fb^{-1} in Phase-2 are also given in Table 1.

The increased amount of collected data foreseen for Phase-2 offers us the opportunity to perform the angular analysis in narrower q^2 bins, in order to measure the P'_5 shape as a function of q^2 with finer granularity. The q^2 region below the J/ψ mass (squared), which is more sensitive to possible new physics effects, is considered. Each Run I q^2 bin is split into smaller and equal-size bins trying to achieve a statistical uncertainty of the order of the total systematic uncertainty in the same bin with the additional constraint of having a bin width at least 5 times larger than the dimuon mass resolution σ_r. If both conditions cannot be satisfied, then only the looser requirement on the $5\sigma_r$ bin width is imposed. The dimuon mass resolution is obtained from the MC simulation as a function of q^2. With respect to the Phase-2 systematic uncertainties with wider bins, the systematic uncertainties that were scaled the same as the statistical uncertainties are adjusted to account for less data in each bin while the other systematic uncertainties are unchanged. The resulting binning is given in Table 2, along with the projected statistical and systematic uncertainties. The lower two pads of Fig. 3 show the projected statistical and total uncertainties.

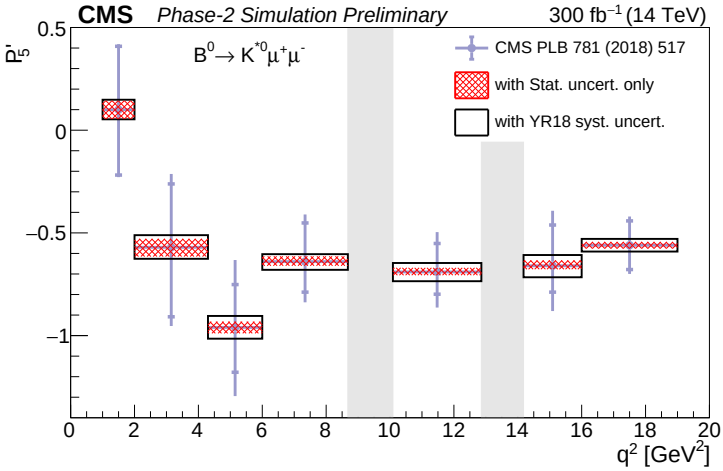

Figure 2: Projected statistical (hatched regions) and total (open boxes) uncertainties on the P'_5 parameter versus q^2 in the Phase-2 scenario with an integrated luminosity of 300 fb^{-1}. The CMS Run I measurement of P'_5 is shown by circles with inner vertical bars representing the statistical uncertainties and outer vertical bars representing the total uncertainties. The vertical shaded regions correspond to the J/ψ and ψ' resonances.

6 Conclusions

The large amount of data expected from the HL-LHC will allow CMS to investigate rare B physics decay channels and, in particular, precisely measure the P'_5 parameter shape in the $B^0 \to K^{*0}\mu^+\mu^-$ mode through an angular analysis. With the large data set of 3000 fb^{-1}, corresponding to around 700K fully reconstructed $B^0 \to K^{*0}\mu^+\mu^-$ events, the P'_5 uncertainties in the q^2 bins are estimated to improve by up to a factor of 15 compared to the CMS measurement from 20 fb^{-1} of 8 TeV data. We also studied the possibility to perform the analysis of the angular observables in narrower q^2 bins, as a better determination of the P'_5 parameter shape will allow significant tests for both beyond Standard Model physics and between different Standard Model calculations. The future sensitivity of the P'_5 angular variable has been presented, however it is worth mentioning that, with the foreseen HL-LHC high statistics, CMS will have the capability to perform a full angular analysis of the $B^0 \to K^{*0}\mu^+\mu^-$ decay mode.

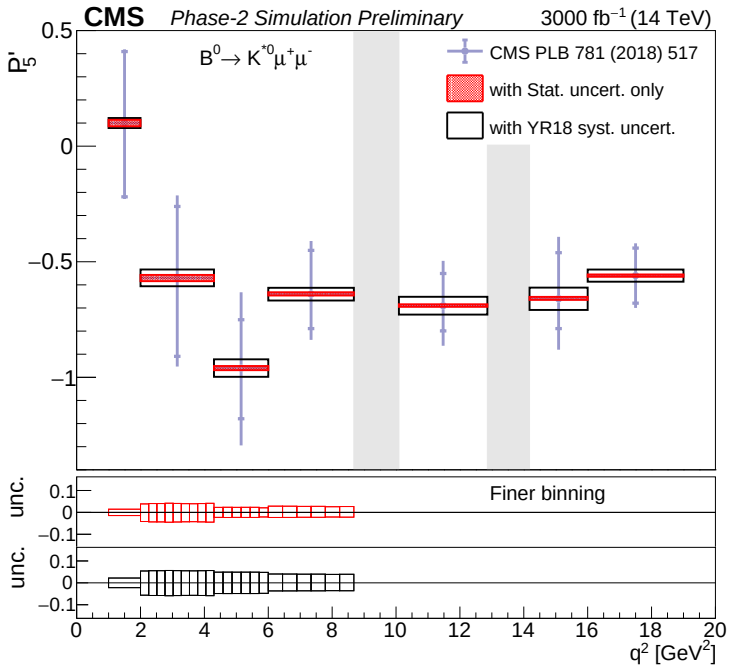

Figure 3: Projected statistical (hatched regions) and total (open boxes) uncertainties on the P_5' parameter versus q^2 in the Phase-2 scenario with an integrated luminosity of 3000 fb^{-1}. The CMS Run I measurement of P_5' is shown by circles with inner vertical bars representing the statistical uncertainties and outer vertical bars representing the total uncertainties. The vertical shaded regions correspond to the J/ψ and ψ' resonances. The two lower pads represent the statistical (upper pad) and total (lower pad) uncertainties with the finer q^2 binning.

Table 1: Statistical and systematic uncertainties in each q^2 bin from the Run I measurement [6] and the HL-LHC extrapolation to 3000 fb^{-1}.

q^2 bin (GeV^2)	Run I	Phase-2
$1.00 < q^2 < 2.00$	$\sigma_{\text{stat}} = ^{+0.32}_{-0.31}$ $\sigma_{\text{syst}} = \pm 0.07$	$\sigma_{\text{stat}} = \pm 0.014$ $\sigma_{\text{syst}} = \pm 0.017$
$2.00 < q^2 < 4.30$	$\sigma_{\text{stat}} = ^{+0.34}_{-0.31}$ $\sigma_{\text{syst}} = \pm 0.18$	$\sigma_{\text{stat}} = ^{+0.014}_{-0.013}$ $\sigma_{\text{syst}} = \pm 0.034$
$4.30 < q^2 < 6.00$	$\sigma_{\text{stat}} = ^{+0.22}_{-0.21}$ $\sigma_{\text{syst}} = \pm 0.25$	$\sigma_{\text{stat}} = \pm 0.009$ $\sigma_{\text{syst}} = \pm 0.037$
$6.00 < q^2 < 8.68$	$\sigma_{\text{stat}} = ^{+0.15}_{-0.19}$ $\sigma_{\text{syst}} = \pm 0.13$	$\sigma_{\text{stat}} = ^{+0.006}_{-0.008}$ $\sigma_{\text{syst}} = \pm 0.026$
$10.09 < q^2 < 12.86$	$\sigma_{\text{stat}} = ^{+0.11}_{-0.14}$ $\sigma_{\text{syst}} = \pm 0.13$	$\sigma_{\text{stat}} = ^{+0.005}_{-0.006}$ $\sigma_{\text{syst}} = \pm 0.038$
$14.18 < q^2 < 16.00$	$\sigma_{\text{stat}} = ^{+0.13}_{-0.20}$ $\sigma_{\text{syst}} = \pm 0.18$	$\sigma_{\text{stat}} = ^{+0.005}_{-0.008}$ $\sigma_{\text{syst}} = \pm 0.048$
$16.00 < q^2 < 19.00$	$\sigma_{\text{stat}} = \pm 0.12$ $\sigma_{\text{syst}} = \pm 0.07$	$\sigma_{\text{stat}} = \pm 0.005$ $\sigma_{\text{syst}} = \pm 0.026$

Table 2: Projected statistical and systematic uncertainties from 3000 fb^{-1} HL-LHC with finer q^2 binning in the low q^2 region.

Run I q^2 bin (GeV^2)	Finer q^2 bin (GeV^2)	Stat. uncertainty	Syst. uncertainty
$1.00 < q^2 < 2.00$	$1.00 < q^2 < 2.00$	$\sigma_{\text{stat}} = \pm 0.014$	$\sigma_{\text{syst}} = \pm 0.017$
$2.00 < q^2 < 4.30$	$2.00 < q^2 < 2.26$	$\sigma_{\text{stat}} = \pm 0.042$	$\sigma_{\text{syst}} = \pm 0.038$
	$2.26 < q^2 < 2.51$	$\sigma_{\text{stat}} = \pm 0.044$	
	$2.51 < q^2 < 2.77$	$\sigma_{\text{stat}} = \pm 0.044$	
	$2.77 < q^2 < 3.02$	$\sigma_{\text{stat}} = \pm 0.045$	
	$3.02 < q^2 < 3.28$	$\sigma_{\text{stat}} = \pm 0.044$	
	$3.28 < q^2 < 3.53$	$\sigma_{\text{stat}} = \pm 0.043$	
	$3.53 < q^2 < 3.79$	$\sigma_{\text{stat}} = \pm 0.043$	
	$3.79 < q^2 < 4.04$	$\sigma_{\text{stat}} = \pm 0.043$	
	$4.04 < q^2 < 4.30$	$\sigma_{\text{stat}} = \pm 0.045$	
$4.30 < q^2 < 6.00$	$4.30 < q^2 < 4.58$	$\sigma_{\text{stat}} = \pm 0.023$	$\sigma_{\text{syst}} = \pm 0.043$
	$4.58 < q^2 < 4.87$	$\sigma_{\text{stat}} = \pm 0.023$	
	$4.87 < q^2 < 5.15$	$\sigma_{\text{stat}} = \pm 0.023$	
	$5.15 < q^2 < 5.43$	$\sigma_{\text{stat}} = \pm 0.023$	
	$5.43 < q^2 < 5.72$	$\sigma_{\text{stat}} = \pm 0.023$	
	$5.72 < q^2 < 6.00$	$\sigma_{\text{stat}} = \pm 0.021$	
$6.00 < q^2 < 8.68$	$6.00 < q^2 < 6.45$	$\sigma_{\text{stat}} = \pm 0.028$	$\sigma_{\text{syst}} = \pm 0.029$
	$6.45 < q^2 < 6.89$	$\sigma_{\text{stat}} = \pm 0.028$	
	$6.89 < q^2 < 7.34$	$\sigma_{\text{stat}} = \pm 0.027$	
	$7.34 < q^2 < 7.79$	$\sigma_{\text{stat}} = \pm 0.028$	
	$7.79 < q^2 < 8.23$	$\sigma_{\text{stat}} = \pm 0.026$	
	$8.23 < q^2 < 8.68$	$\sigma_{\text{stat}} = \pm 0.027$	

References

[1] A. G. et al., "High-Luminosity Large Hadron Collider (HL-LHC): Technical Design Report V. 0.1". CERN Yellow Reports: Monographs. CERN, Geneva, 2017.

[2] S. Descotes-Genon, L. Hofer, J. Matias, and J. Virto, "Global analysis of $b \to s\ell\ell$ anomalies", *JHEP* **06** (2016) 092, doi:10.1007/JHEP06(2016)092, arXiv:1510.04239.

[3] J. Matias, F. Mescia, M. Ramon, and J. Virto, "Complete Anatomy of $\bar{B}_d \to \bar{K}^{*0}(\to K\pi)l^+l^-$ and its angular distribution", *JHEP* **04** (2012) 104, doi:10.1007/JHEP04(2012)104, arXiv:1202.4266.

[4] LHCb Collaboration, "Angular analysis of the $B^0 \to K^{*0}\mu^+\mu^-$ decay using 3 fb^{-1} of integrated luminosity", *JHEP* **02** (2016) 104, doi:10.1007/JHEP02(2016)104, arXiv:1512.04442.

[5] Belle Collaboration, "Lepton-Flavor-Dependent Angular Analysis of $B \to K^*\ell^+\ell^-$", *Phys. Rev. Lett.* **118** (2017) 111801, doi:10.1103/PhysRevLett.118.111801, arXiv:1612.05014.

[6] CMS Collaboration, "Measurement of angular parameters from the decay $\mathrm{B}^0 \to \mathrm{K}^{*0}\mu^+\mu^-$ in proton-proton collisions at $\sqrt{s} = 8$ TeV", *Phys. Lett. B* **781** (2018) 517, doi:10.1016/j.physletb.2018.04.030, arXiv:1710.02846.

[7] ATLAS, LHCb, CMS Collaboration, E. Graverini, "Flavour anomalies: a review", in *13th International Conference on Beauty, Charm and Hyperons (BEACH2018) Peniche, Portugal, June 17-23, 2018*. 2018. arXiv:1807.11373.

[8] CMS Collaboration, "Technical Proposal for the Phase-II Upgrade of the CMS Detector", Technical Report CERN-LHCC-2015-010. LHCC-P-008. CMS-TDR-15-02, 2015.

[9] CMS Collaboration, "The Phase-2 Upgrade of the CMS Tracker", Technical Report CERN-LHCC-2017-009. CMS-TDR-014, 2017.

[10] CMS Collaboration, "The Phase-2 Upgrade of the CMS Muon Detectors", Technical Report CERN-LHCC-2017-012. CMS-TDR-016, 2017.

[11] CMS Collaboration, "CMS Phase-2 Object Performance", CMS Physics Analysis Summary, in preparation.

[12] CMS Collaboration, "Angular analysis of the decay $B^0 \to K^{*0}\mu^+\mu^-$ from pp collisions at $\sqrt{s} = 8$ TeV", *Phys. Lett. B* **753** (2016) 424, doi:10.1016/j.physletb.2015.12.020, arXiv:1507.08126.

[13] L. Quertenmont, "Particle identification with ionization energy loss in the CMS silicon strip tracker", *Nuclear Physics B (proceedings supplements)* **215** (2011) 95, doi:10.1016/j.nuclphysbps.2011.03.145.

[14] Particle Data Group, M. Tanabashi et al., "Review of particle physics", *Phys. Rev. D* **98** (2018) 030001, doi:10.1103/PhysRevD.98.030001.